Advanced Study of Switchable Spin Crossover Compounds

Gavin Craig

ADVANCED STUDY OF SWITCHABLE SPIN CROSSOVER COMPOUNDS

Universitat de Barcelona

Facultat de Química

Departament de Química Inorgànica

Programa de Doctorat: Química Inorgànica Molecular

Grup de Magnetisme i Molècules Funcionals

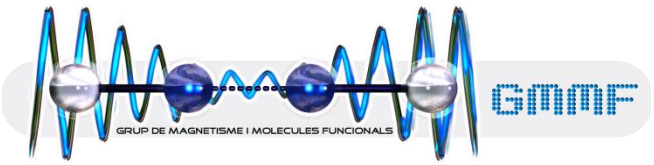

Gavin Craig

Director: Dr. Guillem Aromí Bedmar, Departament de Química Inorgànica

Tutor: Dr. Santiago Alvarez Reverter, Departament de Química Inorgànica

Contents

Chapter 5: Photo-physical properties of the compound $[Fe(H_4L)_2](ClO_4)_2 \cdot H_2O \cdot 2(CH_3)_2CO$ 105

5.0 Introduction 105

5.1 Photo-magnetic properties of 1 (I): LIESST experiments 107

5.2 LIESST versus TIESST: An unexpected discrepancy 110

5.3 Single crystal X-ray diffraction study: Under irradiation 113

5.4 Photo-magnetic properties of 1 (II): Light Induced Thermal Hysteresis 118

5.5 Raman spectroscopy 120

5.6 Excitation within the hysteresis loop on selecting the wavelength of light 123

5.7 Following the pressure-induced SCO by Raman spectroscopy 124

5.8 Concluding remarks 125

5.9 References 127

Chapter 5: Photo-physical properties of the compound $[Fe(H_4L)_2](ClO_4)_2 \cdot H_2O \cdot 2(CH_3)_2CO$

5.0 Introduction

In terms of potential applications, one of the most attractive options for the control of the spin state in Fe(II) spin crossover (SCO) systems[1-4] is the use of light, more commonly known as light induced excited spin state trapping – the LIESST effect (Chapter 1, Section 1.3).[5, 6] This phenomenon was first observed in the solution phase,[7] before Decurtins *et al*. populated the meta-stable HS state of the compound $[Fe(ptz)_6](BF_4)_2$ in the solid state at cryogenic temperatures.[8, 9] It was then discovered that by changing the wavelength of the light source used from the green used for LIESST, to red, the system could be switched from the excited HS state to the ground LS state, labelled the reverse-LIESST effect.[10, 11] The meta-stable character of these excited quintet states leads to their relaxation to the ground singlet state, rendering the precise nature of the involved processes to be of interest, especially when the photo-excitation induces subtle structural differences with respect to the high temperature HS phase,[12, 13] or symmetry breaking within the system.[14-16] The extent of these bi-stable regimes is defined by the temperature *T*(LIESST) (or *T*(TIESST) for a thermal trap), beyond which the HS data generated by photo-excitation is erased.[5] The use of these bi-stable domains is thus hampered by the need to perform the experiments at very low temperatures.

As a way of overcoming this restraint, it was proposed that working within a thermal hysteresis loop could result in a more practical solution, where the photoswitching event would take place within a higher temperature region where the system had proven bi-stability.[17] Though such studies have been carried out on polymeric systems[18-20] and 3D networks,[21-23] Freysz and co-workers were first in describing the phenomenon, for the 0D complex $[Fe(PM\text{-}BiA)_2(NCS)_2]$, demonstrating that a single laser pulse could bring about LS to HS excitation, even if the final state was a mixture of both HS and LS centres.[17] While for this particular compound only the LS to HS conversion could be induced, Liu and co-workers were able to switch bi-directionally within the hysteresis loop for a highly cooperative SCO system based on a macrocyclic ligand.[24] The modification of macroscopic properties that accompanies spin crossover permits the phase transition to be followed via many physical techniques, which for the two highlighted cases were through

changes in reflectivity of the sample, and through absorption spectra, respectively. Another commonplace method to determine the spin state of a system under study is to compare the relative intensities of characteristic bands displayed in Raman spectra.[25, 26]

The drastic decrease in bond lengths on transition from the HS to LS state is reflected by a higher frequency of metal-donor atom vibration in the LS state, such that Raman spectroscopy may give a fingerprint of a system's spin state.[27] Through this approach, Bonhommeau *et al*. could observe reversible photo-switching in the SCO complex [Fe(pyrazine)(Pt(CN)$_4$)].[23] While that study was carried out on a powder sample, Raman spectral mapping of the compound [Fe(bapbpy)(NCS)$_2$] was performed on single crystals,[28] and this flexibility of sample preparation is an advantage of the technique. At the same time, working within the hysteresis loop, or near to it, often entails working close to the temperature of the thermal transition, making it important to be able to distinguish between optical switching and thermal effects.[29]

Raman spectroscopy also allows the SCO process to be followed when it is induced by the application of hydrostatic pressure.[30, 31] The application of an external pressure to a spin crossover system increases the zero point energy difference ΔE_{HL}, which corresponds to the vertical separation of the potential wells that represent the high and low spin states.[32] This decreases the activation energy associated with the HS→LS transition, and drives the HS state towards the denser LS state. This favouring of the LS ground state brings about an increase in the value of $T_{1/2}$ with increasing pressure and, often, a flattening of the crossover.[33]

In Chapter 5, we investigate the photo-physical properties of the 0D SCO compound [Fe(H$_4$L)$_2$](ClO$_4$)$_2$·H$_2$O·2(CH$_3$)$_2$CO (**1**), the thermal SCO properties of which were described in Chapter 4. The possibility of photo-switching the spin state of the compound is probed through LIESST experiments, and the relaxation kinetics are detailed. The crystal structure corresponding to this meta-stable HS state is described, and contrasted with the thermally trapped HS phase characterised in the preceding Chapter. The photo-physical study was then extended to the vibrational spectroscopic properties of **1**, to assess the possibility of performing a photo-switch within the hysteresis loop, while maintaining an awareness of the thermal effects of the laser irradiation. This Raman spectroscopic characterisation is then used to follow the SCO in compound **1** when it is induced by the application of external pressure.

5.1 Photo-magnetic properties of 1 (I): LIESST experiments

LIESST experiments were carried out on **1** in the SQUID magnetometer and the time dependence of χT under irradiation, where χ is the molar magnetic susceptibility, is shown in Figure 5.1. The light source was green, generated by applying LPF500 and SPF650 filters to a Xenon lamp, where LPF means Long Pass Filter, SPF is a Short Pass Filter, and the numbers correspond to the wavelength filtered in nanometres. Initially, two different samples of differing thicknesses were irradiated at 10 K, and the photo-excitation process was observed to be significantly more efficient for the thin sample, an effect ascribed to the penetration depth of the light source. Full excitation to the meta-stable high spin state was achieved for the thin sample after 30 minutes, while the thick sample remains mostly in the LS state.

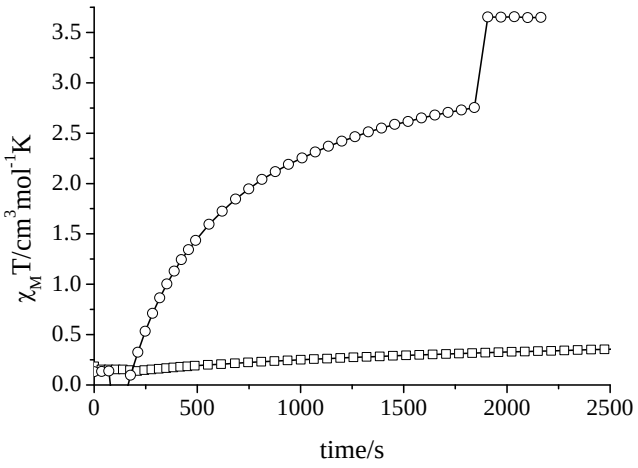

Figure 5.1: Time dependence of χT on irradiation (λ = 500-650 nm). Circles represent the irradiation of a thin crystal sample, and squares represent the irradiation of a thick crystal sample.

Irradiation was then stopped, and the temperature increased at a rate of 1 $Kmin^{-1}$, shown as a χT vs. T plot in Figure 5.2. In the case of the thin sample, the initial value of χT reached at 20 K is 5.02 $cm^3mol^{-1}K$, which leads to a decrease in the magnetic response as the temperature is increased, caused by orientational effects in the crystal sample. Given this phenomenon, a greased sample was used for the χT plot shown in the upper half of Figure 5.2. The initial increase in χT displayed is due to zero field splitting effects, with the magnetic susceptibility reaching a maximum value of 3.10 $cm^3mol^{-1}K$ at 70 K, which is consistent with the 100 % population of the meta-stable HS state (S = 2,

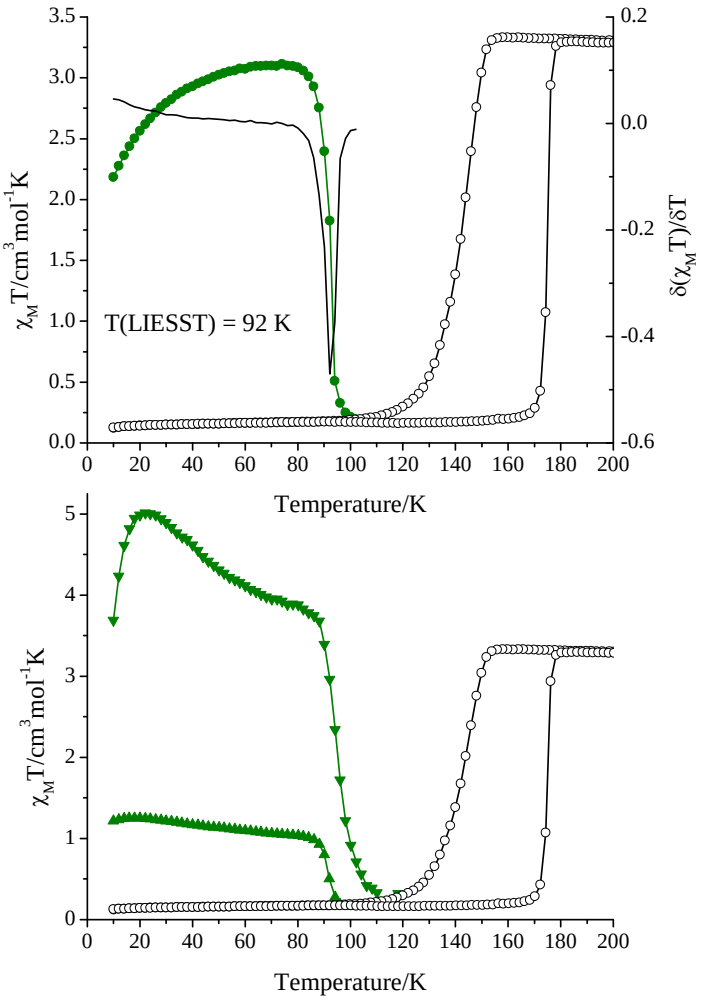

Figure 5.2: χT *vs.* T plots after irradiation at 10 K of **1** (λ = 500-650 nm). (top) The experiment performed on a greased sample. The derivative of this plot yields the value of T(LIESST). (bottom) The irradiation experiments performed on thin and thick crystal samples of **1** (see text for details). The white circles show a thermal cycle performed before LIESST experiments.

χT = 3.0 cm^{3}mol^{-1} K, for g = 2).[34] Above 80 K, the system enters the thermally activated relaxation regime and passes to the diamagnetic LS state. The extent of this bi-stable domain is characterised by the value of T(LIESST), defined by the minimum of the derivative of χT with respect to T, and this parameter is considered to be the temperature above which any HS data induced by the excitation process is erased.[5] For **1**, this measures 92 K (92 and 94 K for the thick and thin samples, respectively), consistent with the inverse energy gap law, and also with the expected value of T(LIESST) based on the value of $T_{1/2}$ for the bis-trichelate nature of the system.[35]

The reverse-LIESST effect allows for the meta-stable HS state to be switched back to the LS state via irradiation at a wavelength other than that used for the initial generation

of the HS state. The results of these experiments on a thin sample are shown in Figure 5.3. Between t = 0 and 2000 s, the HS state is induced through irradiation as before, prior to the filters on the laser being changed to modulate the wavelength of the light which reaches the sample. This process was attempted with two different combinations of filters, however, the values of χT subsequent to irradiation through LPF800 + SPF900 (λ = 800–900 nm) and LPF800 (λ > 800 nm) are consistent with a sample which is still in the HS state, indicating that the sample has not been reversibly photo-switched to the LS state. It could be proposed that the ^5E state into which the HS state is excited through irradiation lies below the $^3T_1$ state, thereby preventing intersystem crossing to the excited singlet states, and leading to relaxation back to the meta-stable $^5T_2$ state (see Figure 1.5 of Chapter 1). It may also be the case that by using band filters to irradiate, there is competition between LIESST and the reverse-LIESST process.

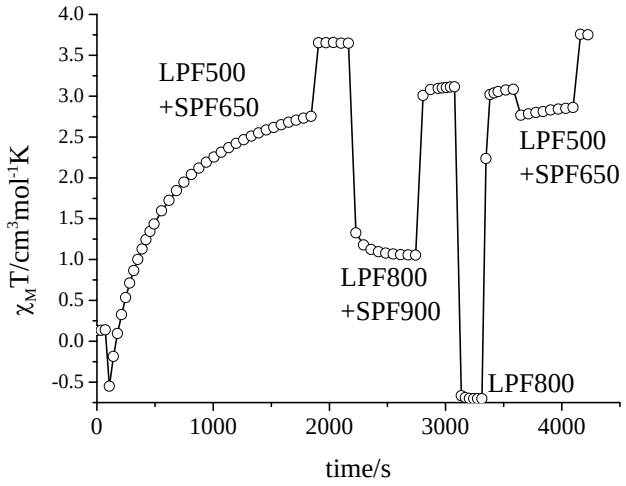

Figure 5.3: Time dependence of χT on irradiation of **1** with different filters.

The relaxation kinetics of the photo-induced meta-stable HS state of **1** were then investigated by measurement of the isothermal time dependence of the fraction of Fe(II) centres in the HS state, γ_{HS} at several different temperatures. To perform these experiments, the system was cooled to 10 K and fully photo-excited to the meta-stable HS state, before being heated rapidly to a series of temperatures below T(LIESST). The trapped HS Fe(II) centres were subsequently allowed to relax from the meta-stable $^5T_2$ state to the ground $^1A_1$ singlet state through a non-adiabatic process.[6, 36] The results of these experiments for compound **1** are shown in Figure 5.4. At the highest temperatures measured, the relaxation was found to begin immediately, while at 82 and 80 K there is a

slight induction period detectable before the HS centres begin to pass to the LS state. The relaxation process involved was modelled with a stretched exponential behaviour that, as in the case of the thermal trapping experiments described in Chapter 4, contrasts with the sigmoidal behaviour normally expected for highly cooperative systems. From these fits, the relaxation rate k_{HL} was obtained for each temperature and used to make the Arrhenius plot shown in Figure 5.4. This analysis yielded a value of the activation energy, E_a, of 1069 cm^{-1} and a rate k_∞ of 20397 s^{-1}. Remarkably, the nature of these relaxation curves is distinct to that observed in the thermal trapping experiments.

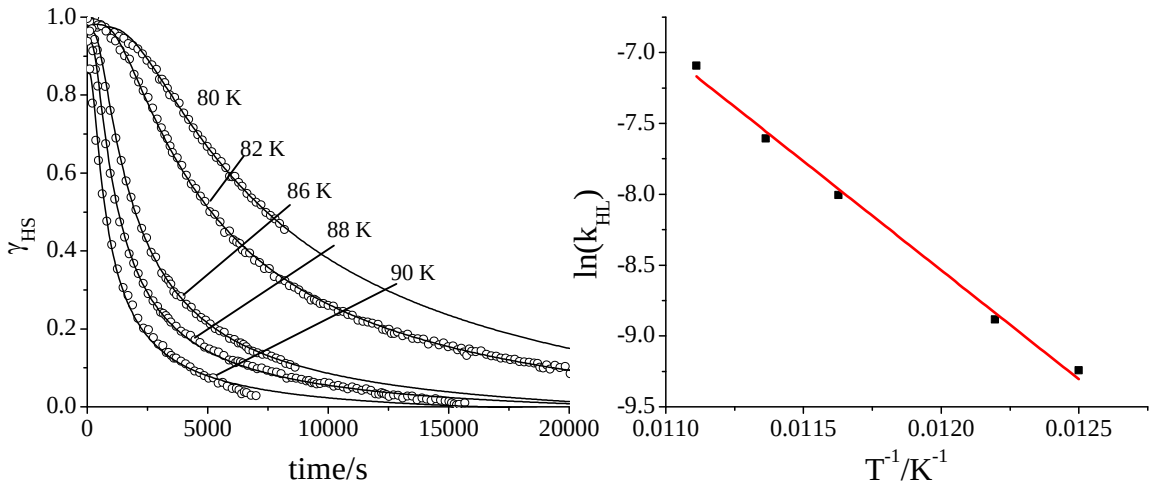

Figure 5.4: (left) High spin fraction γ_{HS} vs. time plot for **1** after LIESST experiments at the temperatures shown. The solid lines represent the fit of the data used to extract the values of k_{HL}. (right) Plot of $\ln(k_{HL})$ vs. $1/T$ based on the relaxation curves.

5.2 LIESST versus TIESST: An unexpected discrepancy

Comparison of the relaxation kinetics at 90 K for both the LIESST and TIESST experiments show that the nature of the relaxation for the LIESST and TIESST phases is clearly different (Figure 5.5). The shape of the TIESST-generated curve is closer to a sigmoidal shape, with an initial period of induction before decay, while the LIESST-generated curve displays an exponential decay. Were both the meta-stable HS phases generated by trapping experiments the same, then similar relaxation processes should be expected.

The intimate relationship between the SCO and order-disorder phase transitions that was demonstrated in Chapter 4 led to the hypothesis that these processes, should they be independent, could cause the observed discrepancy between the relaxation of the meta-

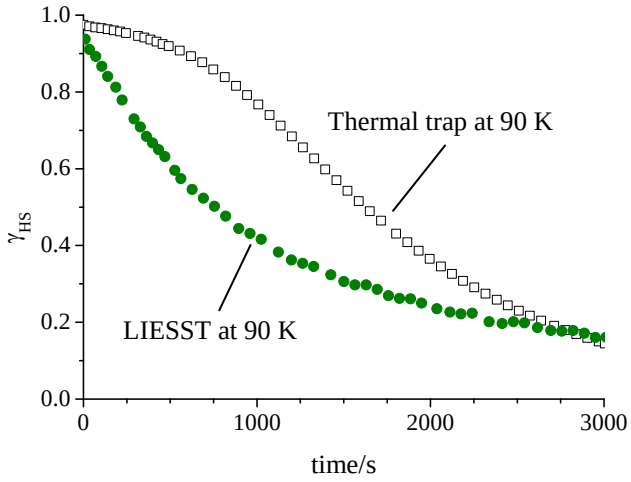

Figure 5.5: High spin fraction γ_{HS} vs. time plot for **1** after LIESST experiments (green) and thermal trapping (white squares) at 90 K.

stable states. To explore this possibility, DSC was employed to characterise the relaxation energetics of the thermally trapped HS state. **1** was flash cooled in liquid nitrogen, before being inserted as quickly as possible in the sample space, which had been pre-cooled to 93 K. The system was then heated at 10 $Kmin^{-1}$, and the heat flow was measured (Figure 5.6). At 119 and 126 K, there are clearly two separate exothermic anomalies in the measurement, though the overall enthalpy change (3.1 $kJmol^{-1}$) is similar to that associated with the thermal HS to LS transition (3.5 $kJmol^{-1}$).

This experimental demonstration that the relaxation of the thermally trapped HS state involves two distinct processes permits the proposition that the isothermal HS→LS

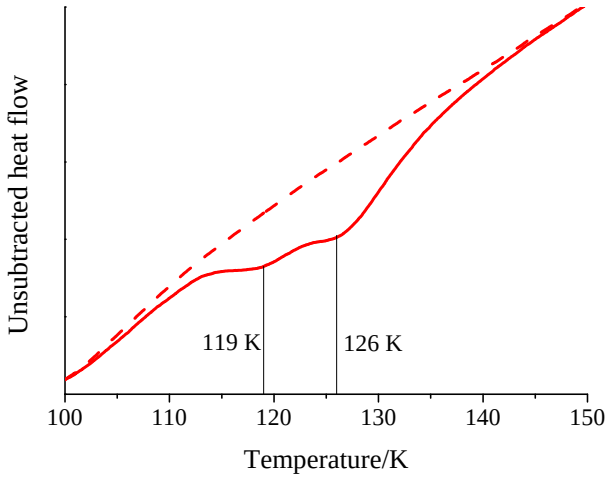

Figure 5.6: Unsubtracted heat flow measurements of **1** in the heating mode after rapid cooling (solid line) and normal cooling (broken line).

transition occurs in two steps: a first, in which perhaps the disordered lattice entities order, leading to the formation of a hypothetical intermediate HS state; and a second, which consists of the transformation of the quintet state into the singlet state. To support this, the relaxation curves were re-interpreted on the basis of a two-step model using Equations 5.1 and 5.2:

$$\gamma_{HS}(t,T) = \gamma_{HS}(t=0,T) \times \exp[-k_{app}(t,T)t] \quad (5.1)$$

$$k_{app}(t,T) = k_{HL}(T) \times [1 - \exp(-k'(T)t)] \quad (5.2)$$

Thus, k_{app} is the apparent relaxation rate of the thermally trapped HS state to the LS state. However, this model allows k_{app} to be deconvoluted into two contributions: k', which is the rate at which the hypothetical intermediate HS state is formed, and k_{HL}, which corresponds to the exponential relaxation of the HS state to the LS state, following Equation 1.8. This model was applied successfully (Figure 5.7, c.f. Figure 4.9) and shows that the k_{HL} values for both the thermally trapped (k_{HL} obtained through the two-step model) and photo-induced meta-stable states (k_{HL} obtained from the stretched exponential fit detailed above) of **1** share a common Arrhenius law (represented by the solid line in Figure 5.7), which yields an activation energy, E_a = 993 cm^{-1} and k_∞ = 5122 s^{-1}. To provide further evidence of this interpretation, the implied structural difference between the photo-excited and thermally trapped meta-stable states needed to be observed.

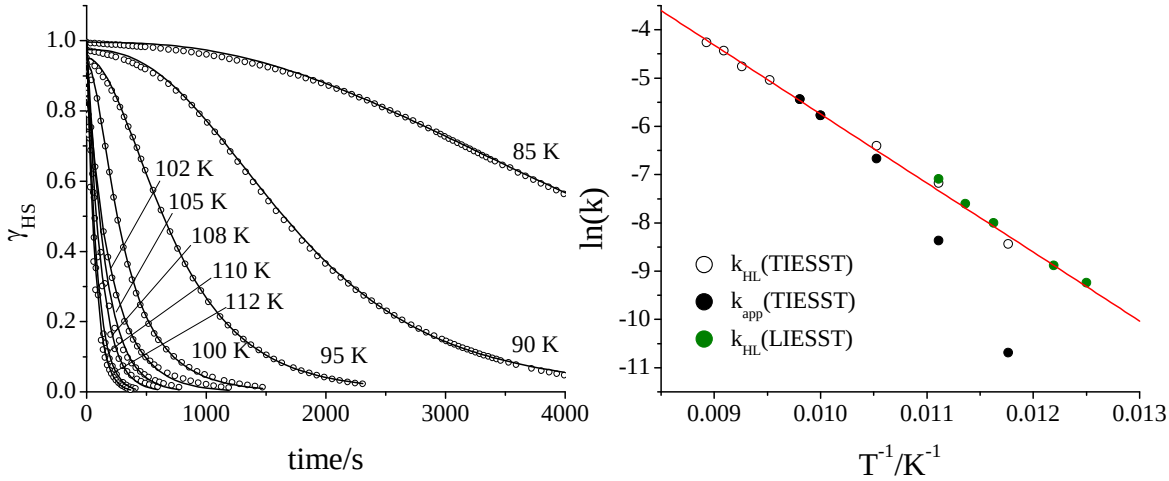

Figure 5.7: (left) Isothermal relaxation experiments after thermal trapping. The solid lines represent the new fits based on the two-step model. (right) Kinetic data for the LIESST and TIESST experiments, following a two step model for the TIESST experiments; the solid line corresponds to a best fit of the k_{HL}(TIESST) data. K_{app} is taken for t = 1000s.

5.3 Single crystal X-ray diffraction study: Under irradiation

In collaboration with the Chemical Crystallography Laboratory at the University of Durham (UK), the crystal structure of the photo-excited meta-stable HS state of **1** (**1**·LIESST) was resolved at 30 K (Table 5.2). The LS→HS transition does not affect the space group or symmetry of the crystals, which remain in the triclinic P_{-1} system. The ligand H_4L retains the same coordination mode to the cation, however the average bond length is larger than that observed at 100 K for the thermally trapped structure: 2.169/2.162 Å (30/100 K), thus, again corresponding clearly to a HS state (see Figure 5.8 and the table for the bond lengths).[4] These longer bond lengths could contribute to the greater degree of distortion observed in the coordination octahedron, reflected by larger values of Σ and Θ, the parameters used to quantify the degree to which the coordination sphere twists away from O_h symmetry to D_{3h} symmetry.[37, 38] Here, they measure 147.90/144.26° and 471.89/464.04°, respectively, perhaps a consequence of the increased bond lengths leading to smaller bite angles around the Fe(II) core. This trend is also observed in the angles θ and Φ, which measure 73.99/74.66° and 176.40/177.05°, respectively.[39] For the photo-generated HS state therefore, the cation is more distorted both in the first coordination sphere and in the shape of the molecule, when compared to the thermally trapped meta-stable HS state.

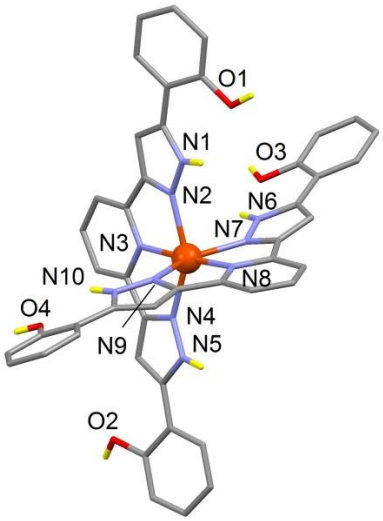

	Bond length/Å	
Bond	**1**·LIESST	**1**·TIESST
Fe-N3	2.141(3)	2.132(3)
Fe-N8	2.120(2)	2.115(3)
Fe-N2	2.160(3)	2.161(3)
Fe-N4	2.177(3)	2.169(2)
Fe-N7	2.206(3)	2.200(2)
Fe-N9	2.212(3)	2.193(3)
Average	2.169	2.162

Figure 5.8 and Table 5.1: View of the $[Fe(H_4L)_2]^{2+}$ cation in **1**·LIESST. Hydrogen atoms omitted for clarity, except those bound to heteroatoms (yellow). Fe-N bond lengths at 30 and 100 K are shown in the table.

Compound	1
	LIESST
T/K	30(2)
crystal system	Triclinic
space group	P-1
a/Å	12.262(5)
b/Å	13.385(5)
c/Å	17.217(5)
α/°	104.127(5)
β/°	98.450(5)
γ/°	106.134(5)
V/Å^3	2561.5(16)
μ/mm^{-1}	0.481
Reflections collected	14451
R1 (all data)	0.0697
wR2 (all)	0.1348
S	1.01
av. Fe-N/Å	2.169
octahedral volume/Å^3	12.508
Σ/°	147.90
Φ/°	176.40(2)
θ/°	73.99
Θ/°	471.89

Table 5.2: Full crystallographic data for the structure of **1** after LIESST at 30 K.

As with the crystal structures described in Chapter 4, the outreaching ligand causes the $[Fe(H_4L)]^{2+}$ cation to favour a crystal packing arrangement predicated on the overlap of adjacent aromatic rings (Figure 5.9).[40] The average distance of these interactions for the HS state of **1** at 200 K is 4.227 Å, and 4.196 Å at 100 K in the thermally trapped HS state. For the photo-generated HS state at 30 K, the average is 4.190 Å, which suggests that the packing of the system within the 2D layers is of similar efficiency, whether the excited state is achieved through irradiation or thermal trapping.

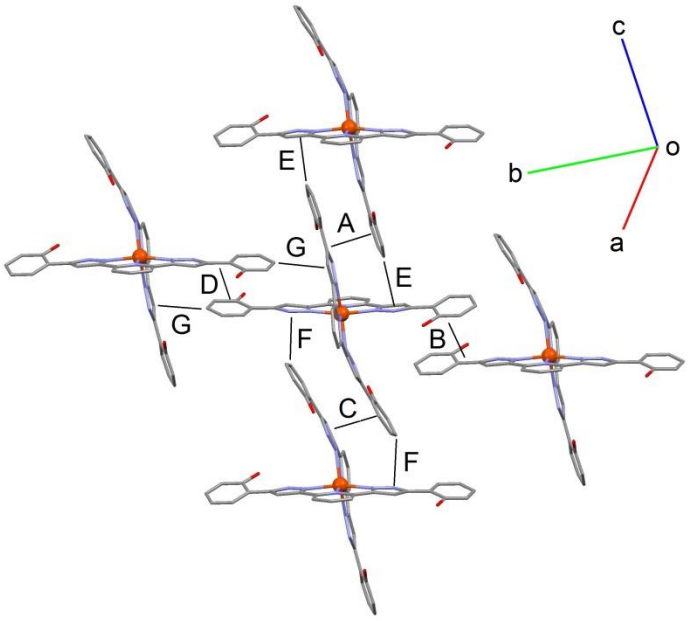

Contact	Type	Distance/Å
A	pz···phen	3.997(2)
B	pz···phen	4.411(3)
C	pz···phen	3.606(2)
D	pz···phen	4.745(3)
E	C44-H44···pz	3.352(4)
F	C27-H27···pz	3.610(4)
G	C21-H21···pz	3.704(4)

Figure 5.9 and Table 5.3: Terpy embrace in **1**·LIESST. The table lists the metric parameters for the contacts involved.

These co-planar cations are then related to each other through the perchlorate anions, acetone molecules, and water molecules that are found in the lattice, which participate in hydrogen bonding motifs. These intermolecular interactions are of the same order as those observed in the previously discussed structures (Figure 5.10). However, there is a significant difference in the disorder observed in the spin-inactive entities in the lattice when compared to the other HS phases. The occupational disorder of half of the perchlorate anions that was discussed in Chapter 4 is absent, as well as that of one of the acetone molecules. In addition, there is a reduction in the level of disorder in the other acetone molecule. This is highlighted in Figure 5.11. Therefore, **1**·LIESST is closer crystallographically than the thermally trapped HS state to the ground LS state.

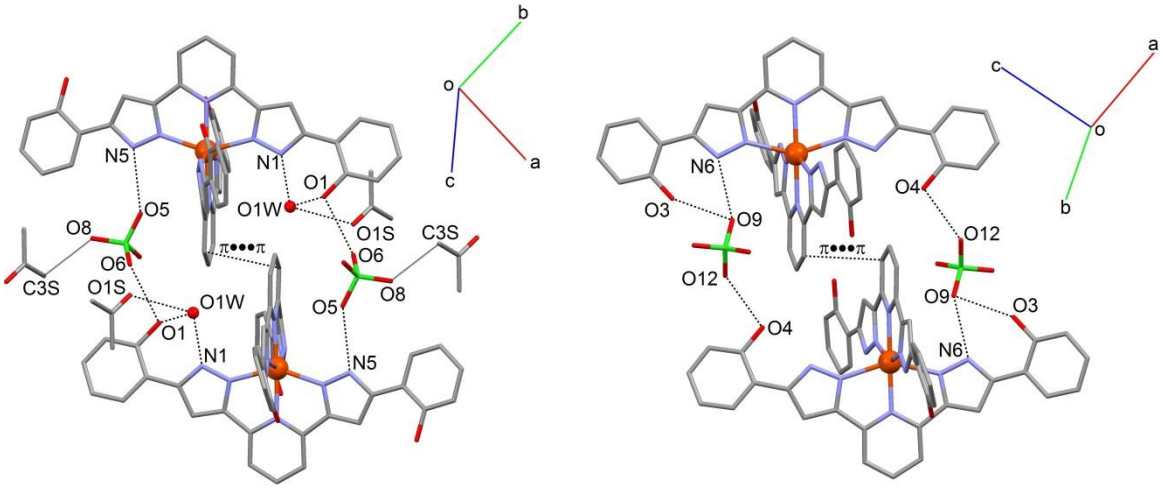

Contact	Distance/Å	Contact	Distance/Å
N1-H1A···O1W	2.844(4)	**N6-H6···O9**	2.880(4)
N5-H5···O5	2.879(4)	**O3-H3···O9**	2.952(4)
O1-H1···O6	2.866(3)	**O4-H4···O12**	2.731(4)
O1-H1···O1W	2.967(3)		
O8···C3S	3.261(8)		
O1S···O1W	2.872(4)		
π···π	4.520(3)	**π···π**	4.807(3)
Fe···Fe	9.925(3)	**Fe···Fe**	9.724(3)

Figure 5.10 and Table 5.4: Hydrogen bonding motifs between layers of the terpy embrace in **1**·LIESST. The table lists the metric parameters for the contacts involved.

Comparison of the unit cells of the meta-stable states and of the ground LS state (Table 5.5), shows that the unit cell parameters of the photo-excited state of **1** closely resemble those of the singlet state, if the thermal contraction along all three axes is considered: a = 12.262/12.326 Å, b = 13.385/13.513 Å, c = 17.217/17.269 Å (**1**·LIESST/LS). The LIESST structure of **1**, therefore, differs in three significant ways from that of the thermally trapped HS state:

- A more highly distorted coordination octahedron.
- A lower degree of structural disorder in the spin-inactive lattice components.
- A unit cell resembling that of the LS state.

As a consequence of the first factor, the potential well of the $^5T_2$ state accessed on irradiation is at a higher energy than that of the thermally trapped meta-stable HS state,

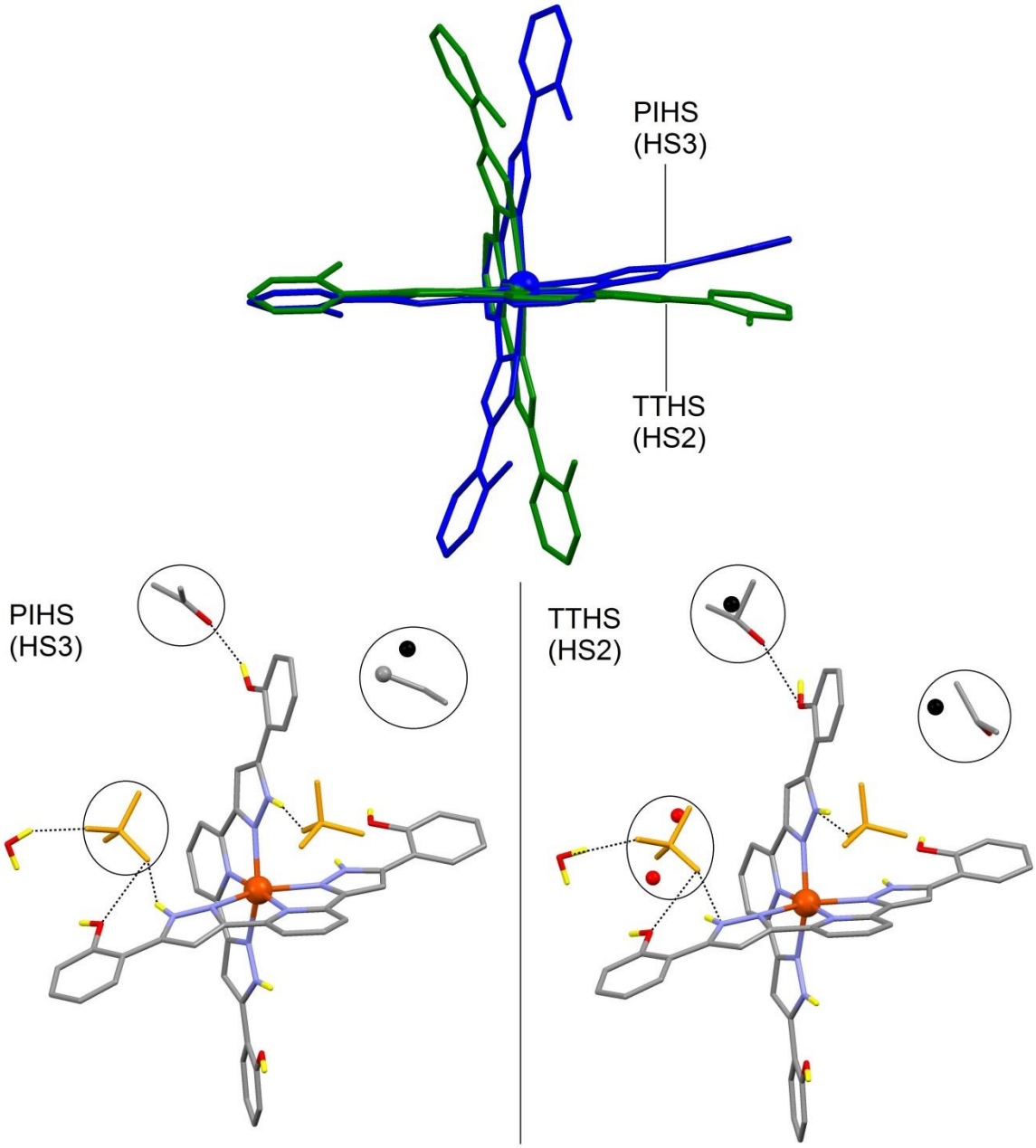

Figure 5.11: (top) Superposition of the $[Fe(H_4L)_2]^{2+}$ cations observed in the LIESST structure (blue, PIHS) and the thermally trapped structure (green, TTHS). (bottom) The lower level of structural disorder in the photo-excited structure highlighted, with the hydrogen atoms omitted for clarity.

leading to a larger zero-point energy difference, $\Delta H^{o}_{HL} = H^{o}_{HS} - H^{o}_{LS}$, which should lead to a faster relaxation of **1**·PIHS to the ground state. However, as shown in Figure 5.7, the relaxation rates observed once the exponential regime have been reached by both systems are of the same magnitude, meaning that at this point the energy difference should be almost the same for both systems. The second and third factors would allow a more

Compound	1			
	PIHS (HS3)	**TTHS(HS2)**	**LS**	**HS**
T/K	30(2)	100(2)	100(2)	200(2)
crystal system	Triclinic			
space group	P-1			
a/Å	12.262(5)	12.247(2)	12.326(3)	12.310(3)
b/Å	13.385(5)	13.385(3)	13.513(3)	13.442(3)
c/Å	17.217(5)	17.355(4)	17.269(4)	17.399(4)
α/°	104.127(5)	104.60(3)	106.63(3)	104.57(3)
β/°	98.450(5)	99.12(3)	98.50(3)	99.29(3)
γ/°	106.134(5)	105.47(3)	106.36(13)	105.44(3)
V/Å^3	2561.5(16)	2574.4(12)	2561.5(13)	2604.1(13)
octahedral volume/Å^3	12.508	12.419	9.741	12.484
Acetone 1 disorder	1:0	0.3:0.7	1:0	0.3:0.7
Acetone 2 disorder (C3S:C3SA)	0.67:0.33	0.4:0.6	1:0	0.4:0.6
ClO_4^- disorder (O9:O9A)	1:0	0.8:0.2	1:0	0.8:0.2

Table 5.5: Selected crystallographic parameters for the three distinct phases observed of compound **1**, after photo-excitation, after thermal trapping, and after slow cooling.

straightforward relaxation to the ground state. The difference in disorder can be rationalised as a consequence of the LIESST process being active on the ordered LS state. Thus, the excitation can be considered as a fast electronic transition that affects the $[Fe(H_4L)_2]^{2+}$ cations, driving them to a HS state in a lattice that is distinct to that obtained on rapidly cooling the high temperature HS state. The unit cell is already that of the LS phase, and concomitant disorder-order transition present in the thermal HS→LS crossover plays a diminished role, explaining the lengthier induction time observed in the relaxation after thermal trapping.

5.4 Photo-magnetic properties of 1 (II): Light Induced Thermal Hysteresis

In systems of sufficiently high cooperativity, it may be possible to observe a hysteresis loop during continuous irradiation: Light Induced Thermal Hysteresis (LITH).[41, 42] This

feature is brought about by competition of, on the one hand, photo-excitation inducing the LS→HS transition and, on the other, simultaneous relaxation from the meta-stable HS to LS ground state.[43] As the temperature is lowered, the relaxation becomes less efficient, to the extent of becoming negligible, and the dominant effect is that of the photo-excitation. The results of this experiment, represented as a χT vs. T curve, are shown in Figure 5.12. The system is cooled at 1 $Kmin^{-1}$ from 200 K to 10 K (blue curve), under constant irradiation. There is a notable distortion of the cooling branch of the hysteresis loop when compared with the thermal transition, before the HS→LS transition is complete at 90 K. The compound **1** remains in the diamagnetic state as the temperature is lowered until around 50 K, where the value of χT begins to increase due to the decreasing rate of relaxation of any meta-stable HS state generated. The magnetic response reaches a maximum value of χT = 3.54 $cm^3mol^{-1}K$ at 14 K, before zero field splitting effects cause the decrease observed at the lowest temperatures measured. In the heating mode, the curve (in red) re-traces that observed in the LIESST experiment for a thin sample, because photo-excitation causes the complete trapping of the HS state, and so, the maximum value of χT. Above 80 K, the thermally activated relaxation of the sample becomes so rapid that the HS→LS transition is observed. The inefficiency of the irradiation above 50 K leads to a broad hysteresis loop induced by the photo-excitation, measuring around 64 K, as derived from the minima observed in the derivatives with respect to temperature of the two χT measurements.

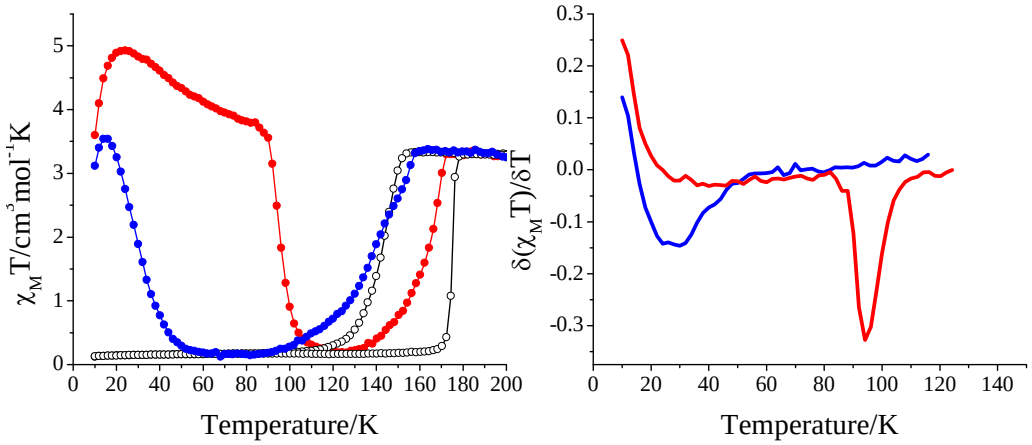

Figure 5.12: (left) LITH experiments shown in the cooling mode (blue) and heating mode (red) under constant irradiation, as a χT vs. T curve. A reference thermal cycle is shown (white circles). (right) First derivative of the χT curves with respect to T for the LITH experiments, from which the width of the hysteresis loop was extracted.

5.5 Raman spectroscopy

Raman spectroscopy has been well-established as a tool for following spin transition processes, whether induced by the variation of temperature,[28, 44, 45] or irradiation with light.[20, 22, 46, 47] Given that milling crystals of **1** leads to a HS sample devoid of SCO behaviour, Raman spectroscopy therefore presents itself as an ideal technique for the characterisation of this system because it allows direct measurement of the sample in the crystal form. Raman studies of compound **1** could be carried out over the course of several placements in the Switchable Molecular Materials group at the Laboratoire de Chimie de Coordination in Toulouse, France. The Raman spectra of compound **1** in the high and low spin states are shown in Figure 5.13. There are characteristic peaks in the high spin spectrum at 1584 and 1024 cm^{-1}. The former disappears on undergoing spin transition, while the latter is displaced to 1033 cm^{-1} in the LS state. This displaced mode is tentatively assigned to the stretching/squeezing of the Fe(II)-N(pyridyl) bond, based on a joint experimental/theoretical Raman study carried out on a system containing a related bis-pyrazolylpyridyl ligand.[48] The peak at 1208 cm^{-1} in the low spin spectrum is unique to the LS spectrum; therefore, the relative populations of the two spin states were calculated using the normalised relative intensities of the peaks at 1024 cm^{-1} for the HS state, and 1208 cm^{-1} for the LS state.

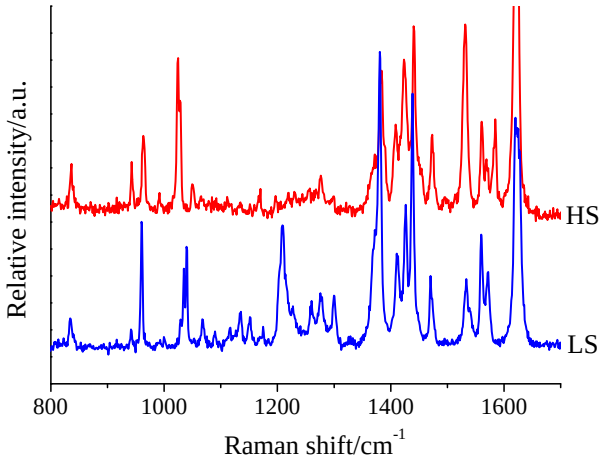

Figure 5.13: Raman spectra corresponding to the HS state of **1** at room temperature (red), and the LS state at 90 K (blue).

An important experimental consideration when performing Raman experiments is the potential for the sample to be locally overheated.[20, 29] This question is particularly important when measurements are taken close to the thermal transition temperature in the

heating mode – it may be the case that a transition is thermally induced by the laser irradiation, rather than through a purely optical effect. In order to gain an appreciation of possible heating effects experienced by the sample when irradiating with both green (λ = 532 nm) and red (λ = 633 nm) light sources, a series of tests were executed, varying the filters employed to attenuate the intensity of the lasers. The first is illustrated in Figure 5.14 showing the experiments carried out at 158 K, irradiating with the red laser (λ = 633 nm). The sample was cooled from the high temperature HS state down to 80 K, inducing a transition to the singlet state, and was then heated to 158 K – 10 K below the onset of the $^1A_1 \rightarrow {}^5T_2$ transition. Irradiation under the D3 filter – the strongest – returns a fully LS spectrum, as evidenced by the strong peak at 1208 cm^{-1} and the absence of a signal at 1584 cm^{-1}. The same was observed on changing to the weaker D2 filter, allowing the conclusion that any heating effect under these conditions is less than the 10 K necessary to bring about the thermal transition. The final spectrum presented in Figure 5.14 is the result of irradiation under the D1 filter, and the absence of a peak at 1208 cm^{-1} is indicative of a HS spectrum, and therefore of a heating effect greater than 10 K. This process was repeated at 163 K (within 5 K of the thermal SCO), and at both 158 and 163 K for irradiation with the green laser (λ = 532 nm). Irradiation with green light at 163 K, indicated a co-existence of both the HS and LS states under both the D3 and D2 filters. This contrasted with the results at 158 K, where a pure LS spectrum was obtained under the D3 filter. Therefore, the experiments to probe for photo-switching were carried out under the D3 filter, precluding the possibility that any light-induced

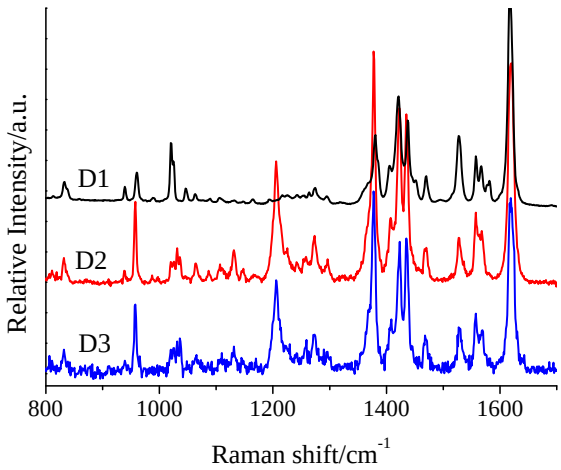

Figure 5.14: Raman spectra obtained for **1** under irradiation with a red laser, λ = 633 nm at 158 K. Three different filters were used: D3 (blue), D2 (red), and D1 (black), from strongest to weakest.

switching be due to heating effects, except at those temperatures within 10 K of the thermal SCO.

The temperature dependence of the spin state of **1** was investigated starting from the LS state at 80 K. A spectrum was collected with the red light source. The temperature was then cycled through to 180 K and back down to 80 K, acquiring a spectrum at 5 K intervals. A qualitative γ(HS) vs. *T* curve was then derived, and the results are presented in Figure 5.15. The obtained cycle approximately coincides with the SQUID Magnetometer data, with the spin transition beginning closer to 140 K than 150 K in the cooling mode, an effect attributable to heating of the crystal, in which the effective temperature at the point where the spectrum is collected is between 5 and 10 K higher than that marked by the cryostat. The transition is apparently complete in nature, and shows an abrupt transition from the LS to HS state near 165 K.

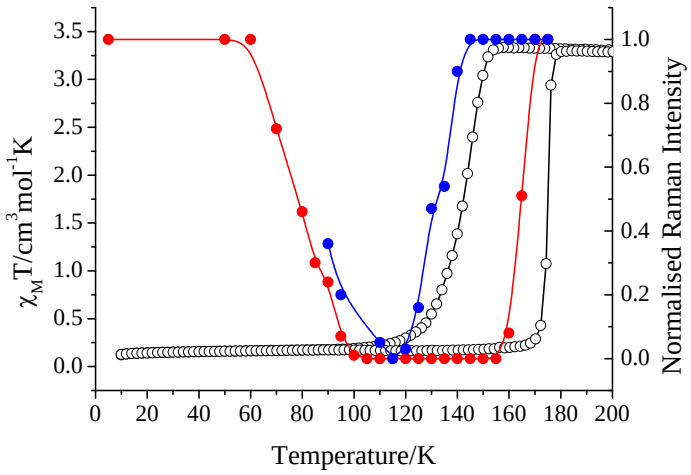

Figure 5.15: Normalised Raman Intensities vs. *T* plot, for the cooling (blue) and heating (red) modes, the solid lines being guides for the eye. The thermal cycle shown by the white circles corresponds to that obtained in the SQUID on a crystal sample of **1**.

The data below 100 K appear to demonstrate the LIESST effect, and the spectra corresponding to 80, 90 and 100 K are presented in Figure 5.16. Using a He cryostat, these experiments were extended to temperatures below that of liquid N_2, enabling measurement of the Raman spectra at 5, 50, 60 and 70 K. The relative intensities of the peaks at 1024 and 1584 cm^{-1} are proof of the loss of efficiency of photo-excitation above 70 K as the temperature is raised.

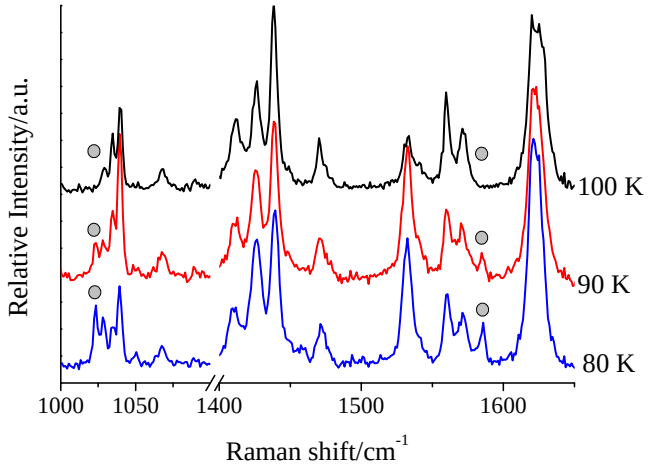

Figure 5.16: Illustration of the diminishing LIESST efficiency on raising the temperature. The grey circles highlight the HS marker peaks.

5.6 Excitation within the hysteresis loop on selecting the wavelength of light

The possibility of photo-switching compound **1** within the hysteresis loop was investigated by first cooling a sample to 78 K and establishing the LS state. At this temperature the crystal was irradiated with red light, yielding a spectrum corresponding to the complex in a mixed HS/LS state (37:63), due to the partial photo-excitation previously observed (Figure 5.17). The light source was changed to the green laser and the sample irradiated again, producing a more complete switch to the metastable HS state (97:3). The compound was then heated to 138 K, a temperature within the bi-stable domain observed in the SQUID measurements. Irradiation with red light demonstrated that the sample was almost entirely in the LS state (10:90). Swapping the light source for the green laser led to the spectrum in Figure 5.17. The appearance of a peak at 1584 cm^{-1} and the absence of the LS indicator peak at 1208 cm^{-1} is proof that a majority HS state has been generated from a LS starting point within the hysteresis loop of compound **1** (95:5). At 138 K, the compound is approximately 30 K below the temperature at which the thermal spin crossover is induced in **1**, which exceeds the extent of the heating effect discussed previously (<10 K under the D3 filter). Therefore, the system has been successfully photo-switched from the singlet state to the triplet state using green light, while the effect is absent when irradiated with red light.

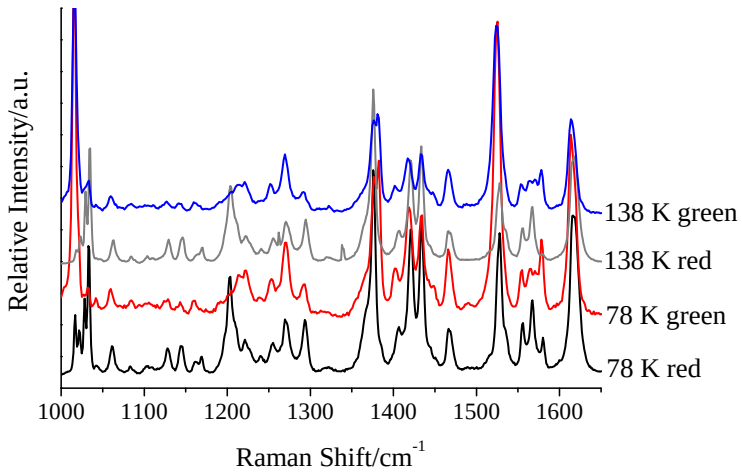

Figure 5.17: Raman spectra obtained at 78 and 138 K via irradiation with either green (λ = 532 nm) or red (λ = 633 nm) light.

5.7 Following the pressure-induced SCO by Raman spectroscopy

As well as allowing the study of the magnetic properties under temperature variation, Raman spectroscopy affords the possibility of monitoring the spin state of Fe(II) compounds under the application of pressure.[30, 31, 33] The sample chamber of a screw-driven diamond anvil cell was filled with a crystal sample of **1**, some ruby chips, and silicone oil which was used as the hydrostatic pressure transmitting medium. The pressure applied via tightening the screws was determined by the ruby fluorescence method, where the displacement of the ruby signal's Raman shift is proportional to the pressure applied.[49] At room temperature, using a red light source, 26 Raman spectra were collected at various pressures in the range 0-34 kbar. A contour map relating the Raman shift with the applied pressure and the relative population of the two possible spin states is shown in Figure 5.18. The x-axis displays the Raman shifts for the signals in the spectra, and as with the study described above, the marker peaks at 1208 cm^{-1} (LS) and 1024 cm^{-1} (HS) were used to determine the spin state of the system. The y-axis displays the pressure applied to the system, such that at atmospheric pressure and room temperature, **1** is found in the HS state, shown by the absence (blue colour in the graph) of a signal at 1208 cm^{-1} and a relative population of the signal at 1024 cm^{-1} of 100% (red colour in the graph). During the initial increase in pressure, the system remains in the HS state, at least until 18 kbar, where the first Fe(II) centres switch to the LS state, with the consequent appearance of the respective marker peak at 1208 cm^{-1}. The intensity of this signal increases with pressure until the SCO process is complete at 23 kbar. Concomitant with the transition to

the LS state is the displacement of the HS signal at 1024 cm^{-1} to 1033 cm^{-1}, as observed above. Due to a design flaw of the pressure cell, releasing the pressure causes a leak of the silicone oil. This prevented the possibility of gradually decreasing the pressure to test for the presence of a piezo-hysteresis loop. Reversibility of the SCO was proven by observation of a HS spectrum after a measurement upon fully returning to atmospheric pressure.

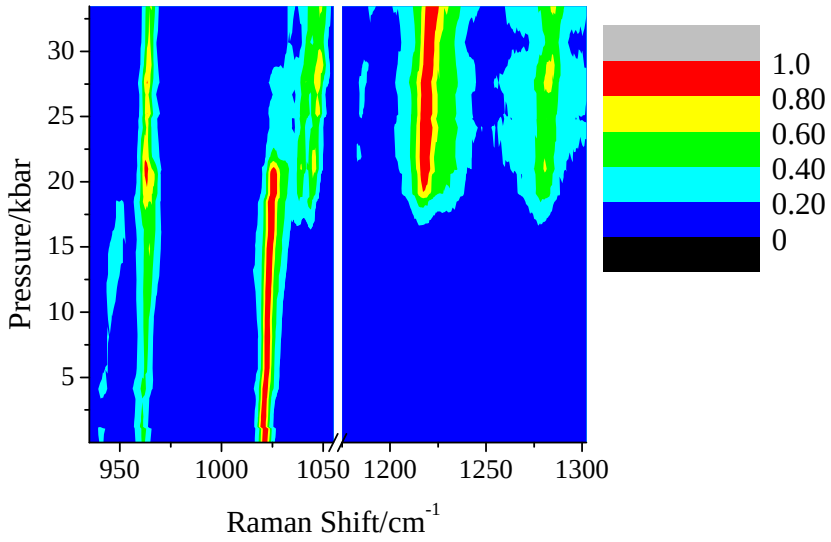

Figure 5.18: Contour map derived from Raman spectra (λ = 633 nm) obtained at room temperature and with increasing pressure.

5.8 Concluding remarks

Both magnetometry and vibrational spectroscopy have been used to demonstrate that by irradiating the 0D SCO compound $[Fe(H_4L)_2](ClO_4)_2 \cdot H_2O \cdot 2(CH_3)_2CO$ (**1**) with red or green light at cryogenic temperatures, the system can be photo-switched from the LS ground state to a meta-stable HS state. This property is vital for potential application of SCO compounds in a practical setting.[2, 50] Unusually, the photo-generated meta-stable state was observed to display different relaxation kinetics to the thermally trapped state, leading to the postulation and reinterpretation of the latter phase based on a two-step model, whereby an initial slow step occurs before a relaxation process of similar rate to that seen in the LIESST state. This hypothesis was reinforced by the presence of two thermodynamic anomalies in the DSC trace upon heating of the thermally trapped phase. Crucially, the crystal structure obtained after the LIESST experiment at 30 K was observed to be not only distinct to the thermally trapped crystal structure, but to

correspond to a *less* disordered phase that was closer in nature to the LS state. This justified the two-step approach to the interpretation of the kinetics, suggesting that the slow step that leads to the induction period in the isothermal relaxation is brought about by an ordering process which leads the thermally trapped phase to a phase similar to that of the photo-trapped one, before both undergo the same relaxation process to the LS ground state. This also is a manifestation of the bearing of factors outwith the first coordination sphere on a system's SCO behaviour, as the level of disorder in the lattice entities plays a vital role in the extent of **1**'s low temperature bi-stable domain.

The accessibility of these meta-stable states was then investigated using Raman spectroscopy, where significant changes in the vibrational spectra were used to determine the spin state of the system. Two key practical aspects were addressed; i) within the hysteresis loop, it was shown that selective generation of the meta-stable HS state could be achieved by varying the wavelength of light employed, and ii) the possibility that any HS data observed were due to heating effects. This second factor allows the assertion that the HS spectra obtained subsequent to irradiation are a genuine consequence of the LIESST effect, and not brought about by local heating of the sample causing the sample to experience a thermal LS→HS crossover, validating the results of the first factor, where green light was shown to be a more efficient method of photo-excitation with respect to red. The comprehensive vibrational characterisation that this studied implied was then used to interpret the effect of applying pressure on **1**. There, the increased pressure favours the denser lower spin state, and a reversible SCO was observed to be induced at room temperature on reaching an external pressure of 23 kbar.

5.9 References

1. A. Bousseksou, G. Molnar, L. Salmon and W. Nicolazzi, *Chem. Soc. Rev.*, 2011, **40**, 3313-3335.
2. P. Gamez, J. S. Costa, M. Quesada and G. Aromí, *Dalton Trans.*, 2009, 7845-7853.
3. P. Gütlich, Y. Garcia and H. A. Goodwin, *Chem. Soc. Rev.*, 2000, **29**, 419-427.
4. P. Gütlich, A. Hauser and H. Spiering, *Angew. Chem. Int. Ed.*, 1994, **33**, 2024-2054.
5. J. F. Létard, *J. Mater. Chem.*, 2006, **16**, 2550-2559.
6. A. Hauser, *Top. Curr. Chem.*, 2004, **234**, 155-198.
7. J. J. McGarvey and I. Lawthers, *J. Chem. Soc.-Chem. Commun.*, 1982, 906-907.
8. S. Decurtins, P. Gütlich, K. M. Hasselbach, A. Hauser and H. Spiering, *Inorg. Chem.*, 1985, **24**, 2174-2178.
9. S. Decurtins, P. Gütlich, C. P. Kohler, H. Spiering and A. Hauser, *Chem. Phys. Lett.*, 1984, **105**, 1-4.
10. A. Hauser, *J. Chem. Phys.*, 1991, **94**, 2741-2748.
11. A. Hauser, *Chem. Phys. Lett.*, 1986, **124**, 543-548.
12. V. A. Money, I. R. Evans, M. A. Halcrow, A. E. Goeta and J. A. K. Howard, *Chem. Commun.*, 2003, 158-159.
13. E. J. MacLean, C. M. McGrath, C. J. O'Connor, C. Sangregorio, J. M. W. Seddon, E. Sinn, F. E. Sowrey, S. L. Teat, A. E. Terry, G. B. M. Vaughan and N. A. Young, *Chem.-Eur. J.*, 2003, **9**, 5314-5322.
14. C. H. Shih, C. F. Sheu, K. Kato, K. Sugimoto, J. Kim, Y. Wang and M. Takata, *Dalton Trans.*, 2010, **39**, 9794-9800.
15. N. Bréfuel, E. Collet, H. Watanabe, M. Kojima, N. Matsumoto, L. Toupet, K. Tanaka and J. P. Tuchagues, *Chem.-Eur. J.*, 2010, **16**, 14060-14068.
16. N. Bréfuel, H. Watanabe, L. Toupet, J. Come, N. Matsumoto, E. Collet, K. Tanaka and J. P. Tuchagues, *Angew. Chem.-Int. Ed.*, 2009, **48**, 9304-9307.
17. E. Freysz, S. Montant, S. Létard and J. F. Létard, *Chem. Phys. Lett.*, 2004, **394**, 318-323.
18. G. Galle, D. Deldicque, J. Degert, T. Forestier, J. F. Létard and E. Freysz, *Appl. Phys. Lett.*, 2010, **96**, 3.
19. G. Galle, J. Degert, C. Mauriac, C. Etrillard, J. F. Létard and E. Freysz, *Chem. Phys. Lett.*, 2010, **500**, 18-22.
20. N. O. Moussa, D. Ostrovskii, V. Martinez Garcia, G. Molnar, K. Tanaka, A. B. Gaspar, J. Antonio Real and A. Bousseksou, *Chem. Phys. Lett.*, 2009, **477**, 156-159.
21. S. Bonhommeau, G. Molnar, S. Cobo, D. Ostrovskii and A. Bousseksou, *Polyhedron*, 2009, **28**, 1610-1613.
22. S. Cobo, D. Ostrovskii, S. Bonhommeau, L. Vendier, G. Molnar, L. Salmon, K. Tanaka and A. Bousseksou, *J. Amer. Chem. Soc.*, 2008, **130**, 9019-9024.
23. S. Bonhommeau, G. Molnár, A. Galet, A. Zwick, J. A. Real, J. J. McGarvey and A. Bousseksou, *Angew. Chem.-Int. Ed.*, 2005, **44**, 4069-4073.
24. H. W. Liu, A. Fujishima and O. Sato, *Appl. Phys. Lett.*, 2005, **86**, 122511.
25. J. A. Wolny, R. Diller and V. Schünemann, *Eur. J. Inorg. Chem.*, 2012, **2012**, 2635-2648.
26. W. R. Browne and J. J. McGarvey, *Coord. Chem. Rev.*, 2006, **250**, 1696-1709.

27. J. P. Tuchagues, A. Bousseksou, G. Molnar, J. J. McGarvey and F. Varret, *Top. Curr. Chem.*, 2004, **235**, 85-103.
28. S. Bedoui, G. Molnar, S. Bonnet, C. Quintero, H. J. Shepherd, W. Nicolazzi, L. Salmon and A. Bousseksou, *Chem. Phys. Lett.*, 2010, **499**, 94-99.
29. O. Fouche, J. Degert, G. Jonusauskas, N. Daro, J. F. Letard and E. Freysz, *Phys. Chem. Chem. Phys.*, 2010, **12**, 3044-3052.
30. H. J. Shepherd, P. Rosa, L. Vendier, N. Casati, J.-F. Letard, A. Bousseksou, P. Guionneau and G. Molnar, *Phys. Chem. Chem. Phys.*, 2012, **14**, 5265-5271.
31. H. J. Shepherd, T. Palamarciuc, P. Rosa, P. Guionneau, G. Molnar, J.-F. Letard and A. Bousseksou, *Angew. Chem.-Int. Ed.*, 2012, **51**, 3910-3914.
32. V. Ksenofontov, A. B. Gaspar and P. Gutlich, *Top. Curr. Chem.*, 2004, **235**, 23-64.
33. H. J. Shepherd, S. Bonnet, P. Guionneau, S. Bedoui, G. Garbarino, W. Nicolazzi, A. Bousseksou and G. Molnár, *Phys. Rev. B*, 2011, **84**, 144107.
34. O. Kahn, *Molecular Magnetism, Wiley VCH*, 1993.
35. A. Hauser, *Comments. Inorg. Chem.*, 1995, **17**, 17-40.
36. A. Hauser, A. Vef and P. Adler, *J. Chem. Phys.*, 1991, **95**, 8710-8717.
37. J. K. McCusker, A. L. Rheingold and D. N. Hendrickson, *Inorg. Chem.*, 1996, **35**, 2100-2112.
38. M. G. B. Drew, C. J. Harding, V. McKee, G. G. Morgan and J. Nelson, *J. Chem. Soc., Chem. Commun.*, 1995, 1035-1038.
39. J. M. Holland, J. A. McAllister, C. A. Kilner, M. Thornton-Pett, A. J. Bridgeman and M. A. Halcrow, *J. Chem. Soc. Dalton Trans.*, 2002, 548-554.
40. J. McMurtrie and I. Dance, *CrystEngComm*, 2005, **7**, 216-229.
41. J.-F. Létard, P. Guionneau, L. Rabardel, J. A. K. Howard, A. E. Goeta, D. Chasseau and O. Kahn, *Inorg. Chem.*, 1998, **37**, 4432-4441.
42. A. Desaix, O. Roubeau, J. Jeftic, J. G. Haasnoot, K. Boukheddaden, E. Codjovi, J. Linares, M. Nogues and F. Varret, *Eur. Phys. J. B*, 1998, **6**, 183-193.
43. F. Varret, K. Boukheddaden, E. Codjovi, C. Enachescu and J. Linares, *Top. Curr. Chem.*, 2004, **234**, 199-229.
44. G. Brehm, M. Reiher, B. Le Guennic, M. Leibold, S. Schindler, F. W. Heinemann and S. Schneider, *J. Raman. Spec.*, 2006, **37**, 108-122.
45. G. Molnar, A. Bousseksou, A. Zwick and J. J. McGarvey, *Chem. Phys. Lett.*, 2003, **367**, 593-598.
46. A. Ahrens-Botzong, K. Muffler, S. M. Stuppy, S. Rackwitz, R. Rueffer, V. Schuenemann and J. A. Wolny, in *International Conference on the Applications of the Mossbauer Effect*, 2010.
47. N. Suemura, M. Ohama and S. Kaizaki, *Chem. Commun.*, 2001, 1538-1539.
48. M. Cavallini, I. Bergenti, S. Milita, J. C. Kengne, D. Gentili, G. Ruani, I. Salitros, V. Meded and M. Ruben, *Langmuir*, 2011, **27**, 4076-4081.
49. G. J. Piermarini, S. Block, J. D. Barnett and R. A. Forman, *J. App. Phys.*, 1975, **46**, 2774-2780.
50. J. F. Létard, P. Guionneau and L. Goux-Capes, *Top. Curr. Chem.*, 2004, **235**, 221-249.